EDGE ARTICLE

M$_{12}$L$_{24}$ nanospheres as supramolecular templates for the controlled synthesis of Ir-nanoclusters and their use in the chemo-selective hydrogenation of nitro styrene†

Lotte L. Metz, [a] Rens Ham, [a] Eduard O. Bobylev,[a] Kelly J. H. Brouwer, [b] Alfons van Blaaderen,[b] Rim C. J. van de Poll,[c] Victor R. Drozhzhin,[c] Emiel J. M. Hensen [c] and Joost N. H. Reek [*a]

Controlled preparation of ultrafine metal nanoclusters (<2 nm) is challenging, yet important as the properties of these clusters are inherently linked to their size and local microenvironment. In the present work, we report the utilization of supramolecular pre-organization of organometallic complexes within well-defined M$_{12}$L$_{24}$ coordination spheres for the controlled synthesis of ultrafine Ir nanoclusters by reduction with molecular hydrogen. For this purpose, 24 sulfonate functionalized N-heterocyclic carbene (NHC) Ir complexes (**Ir-s**) were bound within a well-defined M$_{12}$L$_{24}$ nanosphere that is equipped with 24 guanidinium binding sites (**G-sphere**). Reduction of these pre-organized metal complexes by hydrogenation led to the templated formation of nanoclusters with a narrow size distribution (1.8 $\pm$ 0.4 nm in diameter). It was demonstrated through ^{1}H-DOSY-NMR and HAADF-STEM-EDX experiments that the resulting nanoclusters reside within the nanospheres. The reduction of similar non-encapsulated metal complexes in the presence of nanosphere systems (**Ir-s + M-sphere** or **Ir-p + G-sphere**) resulted in larger particles with a broader size distribution (2.3 $\pm$ 2.1 nm and 6.6 $\pm$ 3.2 nm for **Ir-s + M-sphere** and **Ir-p + G-sphere** respectively). The encapsulated nanoclusters were used as a homogeneous catalyst in the selective hydrogenation of 4-nitrostyrene to 4-ethylnitrobenzene and display absolute selectivity, which is even maintained at full conversions, whereas the larger non-encapsulated clusters were less selective as these also showed reduction of the nitro functionality.

Introduction

The preparation and study of ultrafine nanoclusters (NCs) is a topic of increasing interest in various fields. NCs are defined as nanoparticles with a size of ≤2 nm.[1,2] As a result of their high surface-to-volume atom ratio, particles of such minute dimensions exhibit unique physical and chemical properties compared to their larger analogues and bulk materials. Due to their extraordinary properties, these materials have made their way into various applications such as solid-state memory,[3] sensing/imaging[4–7] and catalysis.[7–9] The size, dispersion and surface environment of nanoparticles and nanoclusters are key

to their unique physical properties and catalytic features. Subtle changes can result in substantial differences in their electronic and geometric properties. Therefore, it is of considerable interest to develop methodologies to make nanoclusters with precise control over these properties.[1,2]

In the past decades, various strategies have been reported to gain synthetic control over the size, shape and distribution including the use of biphasic systems[10,11] and dendrimers.[12,13] More recently, templated strategies involving porous materials such as covalent organic frameworks (COFs),[14–17] porous organic cages (POCs)[18–32] and discrete coordination-spheres[33–42] have been emerging.[43–46] Such porous templates can provide a protective cavity for nanoparticle synthesis by sterically impeding certain growth modes, limiting particle aggregation and enhancing particle stability, solubility and size control.[47]

Recently, our group has developed a method for organometallic catalyst encapsulation within well-defined M$_{12}$L$_{24}$ coordination spheres (M = Pt^{2+} or Pd^{2+}),[48–53] internally functionalized with guanidinium anchors (Fig. 1, **G-sphere**).[54–56] These guanidinium functional groups were demonstrated to bind strongly to sulfonate-functionalized molecular catalysts and carboxylate-

^{a}Van't Hoff Institute for Molecular Sciences, University of Amsterdam, 1098 XH Amsterdam, The Netherlands. E-mail: j.n.h.reek@uva.nl

^{b}Soft Condensed Matter, Debye Institute for Nanomaterials Science, Utrecht University, Princetonplein 1, 3584 CC, Utrecht, The Netherlands

^{c}Department of Chemical Engineering and Chemistry, Eindhoven University of Technology, 5600 MB Eindhoven, The Netherlands

† Electronic supplementary information (ESI) available: Experimental details, preparation and characterization of the catalyst. See DOI: https://doi.org/10.1039/d4sc06324d
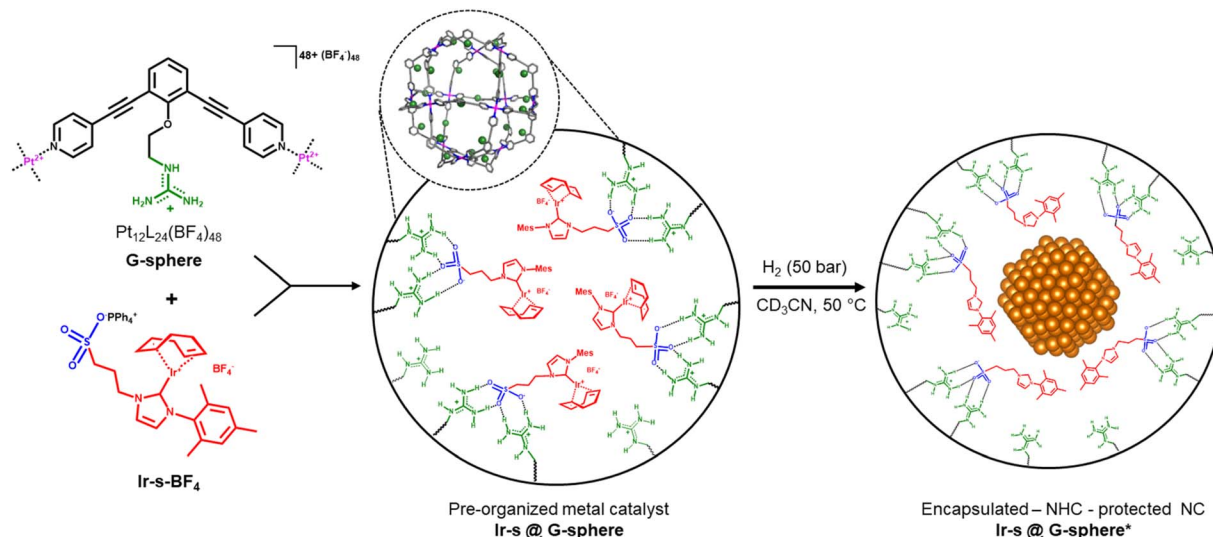
Fig. 1 Schematic representation of the supramolecular pre-organization strategy for controlled nanocluster formation.

functionalized substrates through hydrogen-bonding. This strategy was proven to be a powerful and versatile tool for substrate and catalyst pre-organization and was demonstrated to enhance the catalytic activity and/or selectivity for several homogeneously catalysed transformations.[54–56]

Motivated by the challenges involved in nanocluster synthesis and based on our previous results, we were curious if we could use these nanospheres as templates for confined nanocluster synthesis. It was previously demonstrated that porous microenvironments such as dendrimers,[12,13] COFs[14–17] and POCs[18–32] can limit the growth of nanoparticles prepared from metal salts through steric confinement and by using coordinating functional groups such as amines or sulfides to preorganize metal salts for the initiation of nanoparticle formation. The pre-organization of organometallic complexes in confined space has not been demonstrated and subsequent reduction should lead to the controlled formation of encapsulated nanoclusters that reside in a unique microenvironment in which the ligand of the metal complex precursor may still be present. We herein report the supramolecular pre-organization and reduction of a sulfonate functionalized Ir–NHC complex (**Ir-s-BF$_4$**) within a guanidinium functionalized $M_{12}L_{24}$ sphere (**G-sphere**, Fig. 1). The hydrogenation of encapsulated Ir metal complexes resulted in ultrafine encapsulated nanoclusters (1.8 ± 0.4 nm), which display excellent selectivity in the hydrogenation of 4-nitrostyrene (**1**).

nanoclusters. The metal precursor (**Ir-s-BF$_4$**) was chosen based on three specific requirements: the metal complex should be (1) stable and remain strongly bound to the sulfonate-bearing ligand during encapsulation, (2) readily and cleanly be converted upon reduction by hydrogenation and (3) function as a stabilizing ligand for the resulting nanocluster to retain the cluster within the nanosphere. We anticipated that the N-heterocyclic carbene-based (NHC) metal complex **Ir-s-BF$_4$** would embody these requirements.[57–60]
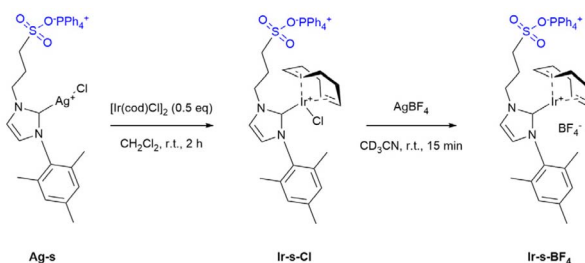
Synthesis of the host (G-sphere) and guest (Ir-s)

The guanidinium functionalized building block (GuaniBB) and corresponding coordination sphere (**G-sphere**) were prepared *via* a modified literature procedure (pages S15–S25†).[54,61] The formation of the $M_{12}L_{24}$ spheres (M = Pt^{2+} or Pd^{2+}) was confirmed with ^{1}H-NMR, DOSY NMR and cold-spray-ionization time-of-flight mass spectrometry CSI-TOF-MS (Fig. S19–S29†), which correspond to previously reported values.[54,55] The sulfonate functionalized iridium complex (**Ir-s-Cl**) was synthesized *via* a modified literature procedure through transmetallation of the corresponding silver carbene (**Ag-s**, Scheme 1).[62] The chloride counter ion of the **Ir-s-Cl** complex was exchanged with BF$_4^-$, to prevent possible compatibility issues of the chloride ions with the Pt$_{12}$L$_{24}$ coordination sphere (**Ir-s-BF$_4$**, Scheme 1).

Results and discussion

Strategy/design of system

The strategy is illustrated in Fig. 1. To start, 24 sulfonated metal complexes (**Ir-s**) should be bound and pre-organized in a well-defined $M_{12}L_{24}$ nanosphere as the sulfonate groups form hydrogen bonds with the 24 guanidinium binding sites located at the inside of the sphere (**G-sphere**). Then, upon subsequent reduction by hydrogenation, these pre-organized metal complexes should lead to the templated formation of

Scheme 1 Synthesis of **Ir-s-BF$_4$**.

The sulfonate functionalized metal complexes (**Ag-s**, **Ir-s-Cl** and **Ir-s-BF$_4$**) were characterized by ^{1}H-NMR, ^{13}C-NMR and CSI-TOF-MS (pages S3–S14†).

Encapsulation of the metal complex

Endohedral binding of **Ir-s-BF$_4$** inside the nanosphere (**G-sphere**) was established by CSI-TOF-MS analysis and various ^{1}H-NMR experiments, which will be discussed in more detail in this section. Direct evidence for the binding of **Ir-s-BF$_4$** was provided by CSI-TOF-MS spectra of a solution of nanosphere in the presence of 8 equivalents of **Ir-s-BF4**, which display multiple charged species that can be assigned to the nanosphere hosting different numbers of **Ir-s** complexes, ranging from 5–9 equivalents of **Ir-s-BF$_4$** per nanosphere (Fig. S44, S45 and Table S2†). It should be noted that under the MS conditions, water coordination and hydrolysis of the carbene ligand to its imidazolium salt is observed, resulting in a variety of encapsulated metal complex/imidazolium salt/H$_2$O combinations (Fig. S46–S49 and Table S3†). As a result, the signals in the MS spectra are substantially broadened obscuring precise interpretation. Consequently, as the number of variations increases with the number of **Ir-s** complexes bound in the nanosphere, the signals become too broad for detection or meaningful interpretation for mixtures containing more than 9 equivalents of complex with respect to the sphere.

Encapsulation was further confirmed by DOSY-NMR (Fig. S36–S39†) of a solution containing 8, 12 or 24 eq. of **Ir-s-BF$_4$** complex with respect to the **G-sphere**, as in such experiment the complex (**Ir-s-BF$_4$**) has signals at the same diffusion as that of the host, in line with encapsulation (Log D = 9.51 m^2 s^{-1} for 8 eq.). In contrast, the free complex in absence of the nanosphere displays a significantly lower diffusion coefficient (Log D = 8.93 m^2 s^{-1}). It should be noted that at full capacity of the host, *i.e.* 24 equivalents of **Ir-s-BF$_4$** with respect to the sphere (Fig. S32 and S34†), there is a subtle increase in the diffusion coefficient for some of the signals of the sphere. This suggests that the hydrodynamic radius of the sphere slightly increases as a result of the crowded interior of the host at full capacity.

To gain more insight into the encapsulation capacity of the host, the binding behaviour was investigated by a titration experiment monitored by ^{1}H-NMR spectroscopy (pages S30 and S31†). In the resulting spectra, the N–H-signal of the endohedral guanidinium functionality (**G-sphere**) most significantly shifts upon introduction of the guest (**Ir-s-BF4$_4$**), whereas the other signals of the sphere display modest to no changes. This result indicates that binding of the guest indeed primarily occurs inside the sphere. A linear correlation between the N–H-signal-shift (**G-sphere**) and guest (**Ir-s-BF$_4$**) concentration was observed up to 18 equivalents of guest. Addition of more equivalents resulted in overlap of peaks, complicating the monitoring of the N–H signal by ^{1}H-NMR spectroscopy (Fig. S42†). This indicates that at least 18 equivalents of **Ir-s** bind to the inside of the **G-sphere**, while they are still able to exchange. Importantly, these experiments combined clearly illustrate the host–guest complexation and anticipated encapsulation capacity of this system.

As a control, we synthesized variations of the nanosphere and metal complex for which the binding element on each side was removed (**M-sphere** and **Ir-p** Fig. 3). Naturally, the lack of encapsulation for both combinations was confirmed by DOSY-NMR and ^{1}H-NMR experiments (Fig. S40 and S41†).

Nanocluster formation

To demonstrate that nanoclusters could be prepared within the nanospheres, reduction of the iridium complexes was performed in the presence and absence of nanospheres. The clusters were prepared by hydrogenation of a 24 : 1 mixture of **Ir-s-BF$_4$** and **G-sphere** to ensure full loading, (1 ml, 8.7 mM, **Ir-s@G-sphere**), and the CD$_3$CN solution was kept at 50 bar H$_2$ and 50 °C for 18 h to allow full reduction. After 18 h, the solution had changed colour from light orange to amber brown and no precipitation was formed, indicating that all iridium was still in solution and no agglomeration had occurred (Fig. 2). The observed colour corresponds to observations reported in literature for small Ir(0) nanoclusters.[63] In contrast, when the **Ir-s-BF$_4$** complex was hydrogenated in absence of the nanosphere, under otherwise identical conditions, precipitates were formed and a dark film was visible on the reaction vessel (Fig. S50†).
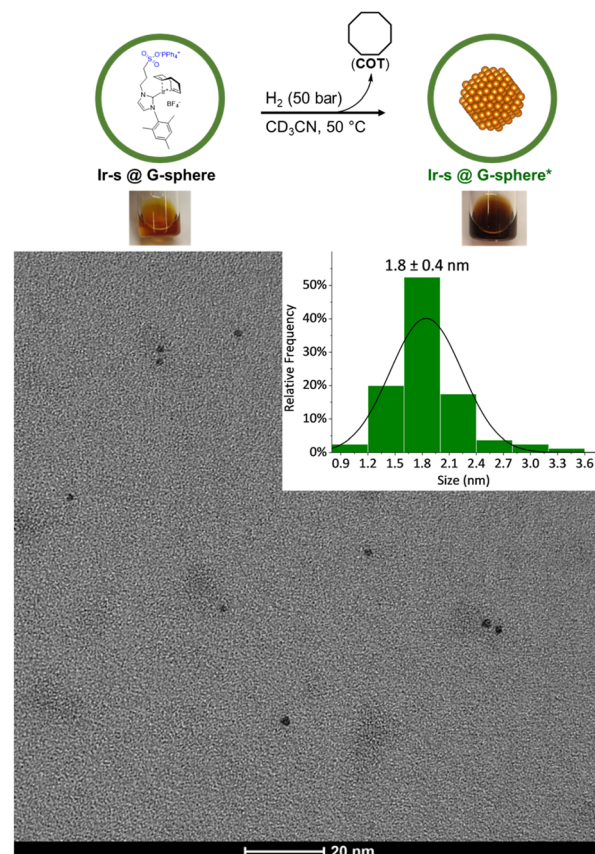

Fig. 2 Top: nanocluster synthesis conditions and representative images of the solutions of **Ir-s@G-sphere** before and after hydrogenation (**Ir-s@G-sphere***) respectively. Bottom: representative TEM image of **Ir-s@G-sphere*** and corresponding size distribution (in diameter).

The dimensions of the Ir clusters formed inside the sphere, were characterized by transmission electron microscopy (TEM). The clusters were determined to be 1.8 ± 0.4 nm in diameter (Fig. 2), which is much smaller than the size of the nanosphere (5 nm).[64,65] However, for nanoparticles consisting of 24 Ir-atoms, a particle size of 0.9 nm would be expected. As the metal complexes are pre-organized in a supramolecular fashion, the **Ir-s-BF₄** complexes can exchange between nanocages, and as this apparently is faster than nanoparticle formation, the final number of Ir-atoms per particle can be larger. Importantly, these results altogether indicate that pre-organization of the **Ir-s-BF₄** within the **G-sphere** results in controlled nanocluster formation (**Ir-s@G-sphere***).

To compare the effects of sphere interaction and encapsulation on cluster size and distribution, the non-encapsulated metal complexes (**Ir-s + M-sphere** and **Ir-p + G-sphere**, Fig. 3) were hydrogenated under otherwise identical conditions. From TEM analysis (Fig. S51 and S52†) it becomes evident that the resulting particle size and distribution for these systems (Fig. 3) are generally larger and significantly broader than the encapsulated clusters (2.3 ± 2.1 nm and 6.6 ± 3.2 nm for **Ir-s + M-sphere** and **Ir-p + G-sphere** respectively). The non-encapsulated sulfonate functionalized metal complex (**Ir-s + M-sphere**) displays a smaller particle size than the non-sulfonated metal complex (**Ir-p + G-sphere**). Importantly, the superior control over the size and size distribution of the encapsulated clusters (**Ir-s@G-sphere**) clearly demonstrates the power of pre-organization.
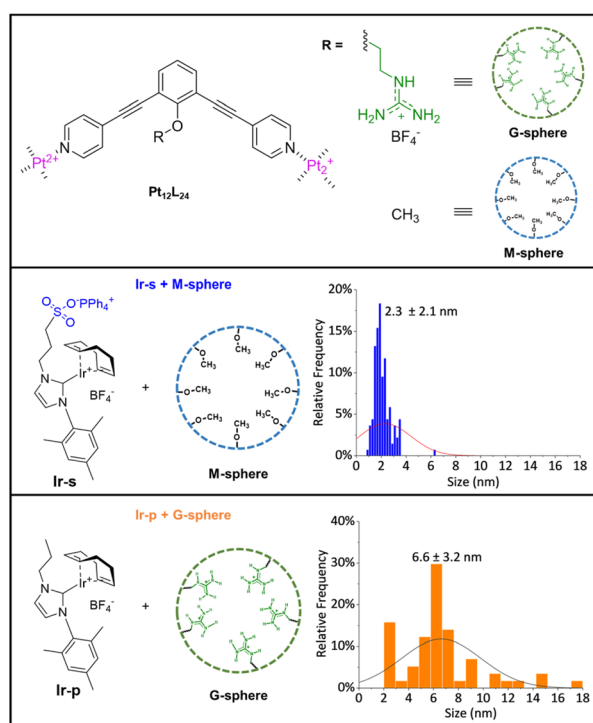

Fig. 3 Schematic representations of control groups and resulting particle size distribution (diameter). Top: schematic representation of **G-sphere** and **M-sphere**, middle and bottom: **Ir-s + M-sphere** and **Ir-p + G-sphere** and corresponding size distribution (in diameter).

To gain further insight into the conversion of the metal precursor and the spatial relationship between the sphere and the encapsulated Ir cluster, the resulting mixture was studied by ^{1}H-NMR and DOSY-NMR. The ^{1}H-NMR spectrum of **Ir-s@G-sphere*** (Fig. S54†) shows the disappearance of the **Ir-s** ligand signals and the formation of its corresponding imidazolium salt, which is expected to form upon nanocluster formation. In addition, the formation of cyclooctane (**COT** at 1.54 ppm) is observed, which is a result of Ir-catalysed hydrogenation of the cyclooctadiene (COD) ligand. Integration of this signal, compared to an internal standard (1,3,5-trimethoxybenzene), confirmed full conversion (Table S4†). Notably, the signals of the nanosphere have become broadened after hydrogenation, which is commonly a result of local restricted motion and the heterogeneous character of the encapsulated Ir clusters.[66] Importantly, the DOSY-NMR spectrum (Fig. 4f) shows that the diffusion coefficient of the encapsulated clusters (**Ir-s@G-sphere***, 9.49 m^2 s^{-1}) remains similar to that of the host–guest system before hydrogenation (**Ir-s@G-sphere**, 9.48 m^2 s^{-1}). These results combined confirm that the nanospheres remain of similar dimensions after nanocluster formation and indicate that the clusters are residing inside the spheres.

The formation of an encapsulated cluster was further evidenced by an energy-dispersive X-ray spectroscopy (EDX) study in combination with high-angle annular dark-field scanning transmission microscopy (HAADF-STEM) imaging (Fig. 4). The images reveal that Ir and Pt are clearly located together, affirming the Ir clusters are indeed encapsulated within the sphere. Moreover, quantification of the Pt and Ir atom fraction through area scanning (Fig. 4c and e) confirmed the 12 : 24 ratio that is expected from the nanosphere – guest system and corresponds to values found with Inductively Coupled Plasma Optical Emission Spectroscopy (ICP-OES) analysis (Table S5†). To further confirm the integrity of the sphere and the formation of metallic Ir nanoclusters in the sphere, the encapsulated systems were studied by XPS analysis before and after hydrogenation conditions that lead to nanoparticle formation (Fig. S59†). The resulting spectra after hydrogenation (**Ir-s@G-sphere***) display two characteristic signals centred around 61.3 eV (Ir 4f$_{7/2}$) and 64.2 eV (Ir 4f$_{5/2}$). These signals were determined to be composed of Ir^0 clusters that are partially oxidized (47% Ir^0), confirming the formation of metallic Ir^0 species under hydrogenation conditions.[67–70] Additionally, the doublets centred around 73.8 eV and 76.8 eV, corresponding to Pt 4f for the Pt^{II} cornerstones of the sphere,[71] remain unchanged after hydrogenation (Fig. S59†). These results confirm that Pt atoms remain unreduced and further support that the sphere remains intact. Overall, these results, combined with the STEM-EDX and DOSY-NMR analyses, clearly demonstrate that the formed Ir^0 nanoclusters are indeed residing within the guanidine containing Pt$_{12}$L$_{24}$ nanospheres.

Catalysis

To evaluate the catalytic activity of the newly formed encapsulated nanoclusters, the hydrogenation of 4-nitrostyrene (**1**) was explored by monitoring the reduction reaction over time (Fig. 5).
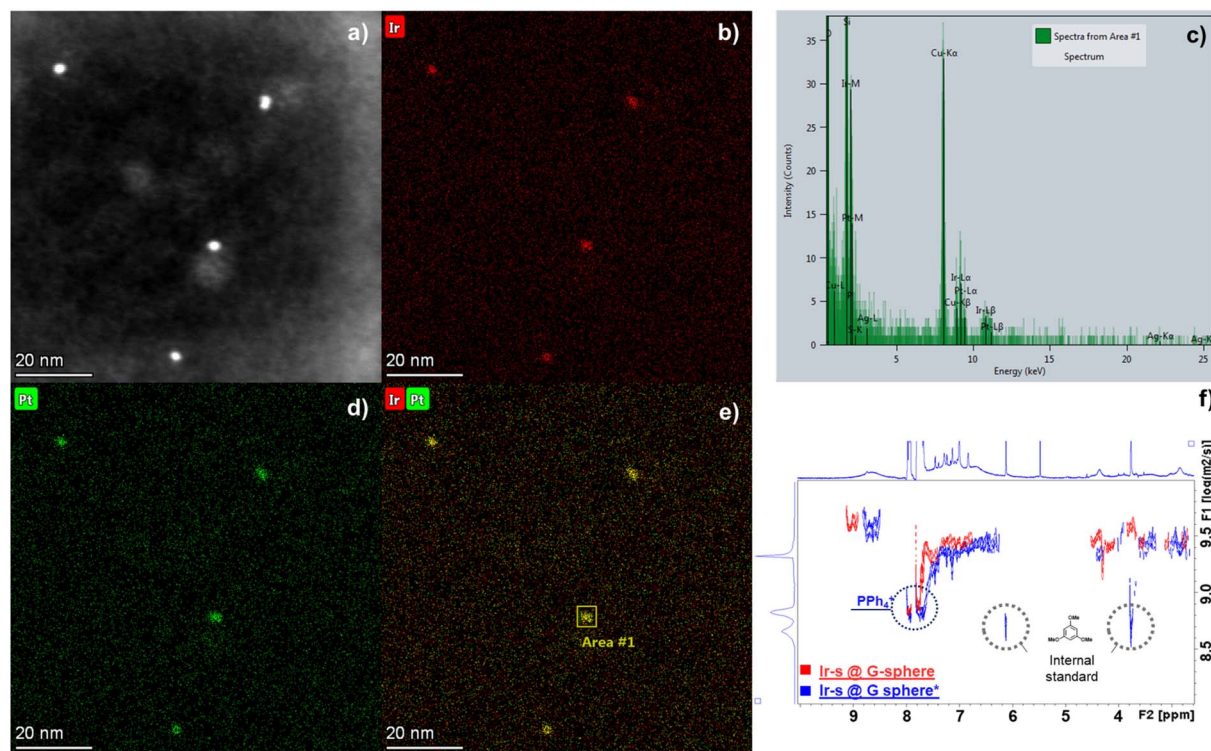
Fig. 4 (a) HAADF–STEM image of **Ir-s@G-sphere*** and corresponding EDX maps of (b) Ir, (d) Pt and (e) an overlay of Ir and Pt, (c) EDX pattern of the selected area in (e), (f) ^{1}H-DOSY-NMR overlay of **Ir-s@G-sphere**/before (red) and **Ir-s@G-sphere***/after hydrogenation.

This reaction was chosen because it can provide insight into both activity and selectivity. For these experiments, the encapsulated and non-encapsulated clusters/NPs (**Ir-s@G-sphere*** and **Ir-s + M-sphere*** respectively) were compared and used as prepared. The hydrogenation reactions were carried out in CH_3CN under hydrogen pressure (50 bar) at 50 °C, using 2 mol% of Ir *vs.* **1**. The product composition was monitored over time by means of GC-MS with an internal standard (Fig. 5). From the observed product compositions, it became evident that both catalytic systems display a preference for alkene reduction, thus favoring the initially selective formation of 4-ethylnitrobenzene (**2**). Notably, the product compositions over time reveal that the **Ir-s@G-sphere*** clusters provide fully selective conversion toward 4-ethylnitrobenzene (**2**) over 17 h (Fig. 5c). In contrast, in the presence of nanoparticles formed by the mixture of **Ir-s + M-sphere***, **1** is rapidly converted to **2** and further reduced to form 4-ethylaniline (**3**) (Fig. 5b). This result highlights a striking difference in catalytic behavior between the encapsulated (**Ir-s@G-sphere***) and non-encapsulated particles (**Ir-s + M-sphere***). Importantly, in the presence of **Ir-s + M-sphere*** over-reduction of **2** to **3** already commences before full conversion is attained (@30 min 66% conversion with 1% of **3**), thus invariably leading to an impure product mixture and a maximum product yield of 87% after two hours (Fig. 5a). On the contrary, in the presence of **Ir-s@G-sphere*** complete conversion to **2** occurs entirely selectively without any observable side product formation even at full conversions. Thus, although **Ir-s + M-sphere*** may be a faster catalyst, **Ir-**

s@G-sphere* eventually provides significantly higher attainable yields. To the best of our knowledge, this is the first iridium nanocatalyst reported to selectively hydrogenate nitrostyrene to ethylnitrobenzene.

To compare the selectivity of **Ir-s@G-sphere*** to nanoclusters with a similar size and size-distribution in a different micro-environment, polyvinylpyrrolidone (PVP) supported Ir-nanoclusters were prepared (**Ir@PVP**) according to a literature protocol.[72] Hydrogenation of **1** under H_2 (40 bar) at 50 °C in the presence of **Ir@PVP** (2 mol%, based on Ir) afforded a mixture of the fully hydrogenated product **3** (4-amino ethylbenzene, 44%) and 4-vinylaniline (<5%). This is in large contrast to the results obtained for **Ir-s@G-sphere*** which resulted in complete and selective conversion of **1** to **2** (4-nitro ethylbenzene), whereas **2** was not observed at all by ^{1}H-NMR nor GC-MS (Fig. S58†) when **Ir@PVP** was used at catalyst. This demonstrates that the unique second coordination sphere around the Ir-nanocluster formed by the cage is crucial for the selectivity displayed by the enclosed nanoparticle. To gain more insight into the role of the guanidinium groups of the **G-sphere** during the catalytic reaction, styrene and 3-vinylbenzoic acid were hydrogenated with **Ir-s@G-sphere***. We anticipated that the guanidinium sites should still be hydrogen bonded to the sulfonate groups from the **Ir-s** ligand. If some of the guanidinium groups would be available for H-bonding, the substrates with carboxylate groups in principle could be pre-organized in close proximity to the nanocluster, and hence should be hydrogenated faster, in line with other previously reported catalytic transformations within the
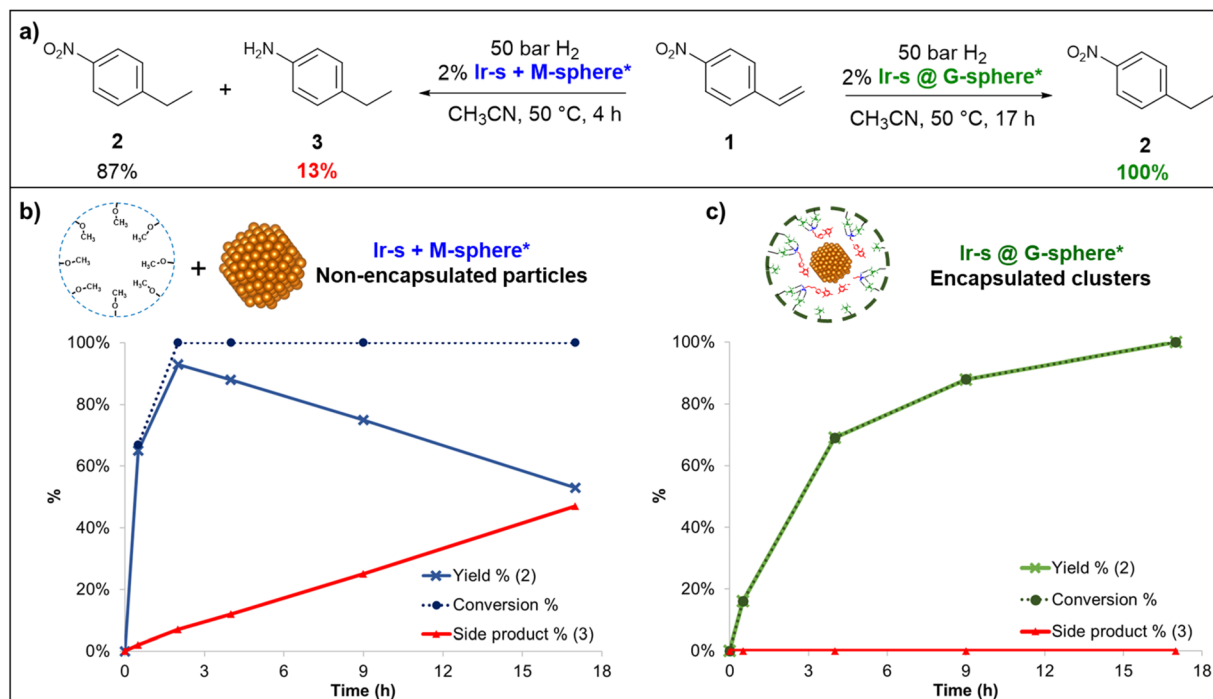
© 2024 The Author(s). Published by the Royal Society of Chemistry

Fig. 5 (a) Hydrogenation of 4-nitrostyrene (**1**): product composition at full conversion in the presence of **Ir-s + M-sphere*** (left) and **Ir-s@G-sphere*** (right), (b) hydrogenation of **1** over time in the presence of **Ir-s + M-sphere*** and (c) in the presence of **Ir-s@G-sphere***. ([**1**] = 60 mM in CH_3CN, 2% Ir $vs.$ **1**).

guanidinium functionalized nanosphere.[54] Although both substrates undergo selective hydrogenation to their ethyl-benzene derivatives, there is no rate acceleration observed for the carboxylate functionalized substrate (Fig. S56†). Apparently, the guanidinium sites are sufficiently engaged in hydrogen bonding to the sulfonate functionalized ligand and thus unavailable for binding additional substrates. Overall, these experiments show that the **Ir-s@G-sphere*** system contains an iridium cluster with a defined size and a unique second coordination sphere, altogether resulting in a selective catalyst for the hydrogenation of nitrostyrene to ethylnitrobenzene.

Conclusions

To summarize, we have demonstrated supramolecular pre-organization in nanospheres as a effective strategy for controlled nanocluster synthesis. We have shown that hydrogenation of the organo-metallic **Ir-s-BF₄** complex encapsulated inside a $Pt_{12}L_{24}$ nano-sphere (**G-sphere**) led to the formation of fine nanoclusters with a narrow size distribution, whereas non-encapsulated precursors did not. These results together demonstrate that pre-organization within the nanosphere can indeed facilitate the templated formation of ultrafine metal nanoclusters. Moreover, we were able to establish that the nanocluster remains encapsulated inside the nanosphere upon formation, underlining that the cluster is indeed formed and stabilized within the sphere. The encapsulated clusters (**Ir-s@G-sphere***) displayed outstanding selectivity in the hydrogenation of 4-nitrostyrene (**1**). We envision this new system can provide

a unique nano environment for nanocluster formation and catalytic conversions, which can be extended to other metals and combinations thereof. Furthermore, we conceive that this preorganization strategy can provide flexibility for subtle ligand modifications and promises to be a versatile tool for controlled synthesis and fine-tuning of small nanoclusters.

Data availability

The datasets supporting this article have been uploaded as part of the ESI.†

Author contributions

Conflicts of interest

There are no conflicts to declare.

Acknowledgements

Notes and references

1 I. Chakraborty and T. Pradeep, *Chem. Rev.*, 2017, **117**, 8208–8271.

2 R. Jin, C. Zeng, M. Zhou and Y. Chen, *Chem. Rev.*, 2016, **116**, 10346–10413.

3 C. Busche, L. Vilà-Nadal, J. Yan, H. N. Miras, D.-L. Long, V. P. Georgiev, A. Asenov, R. H. Pedersen, N. Gadegaard, M. M. Mirza, D. J. Paul, J. M. Poblet and L. Cronin, *Nature*, 2014, **515**, 545–549.

4 L. Y. Chen, C. W. Wang, Z. Yuan and H. T. Chang, *Anal. Chem.*, 2015, **87**, 216–229.

5 P. Chakraborty, A. Nag, A. Chakraborty and T. Pradeep, *Acc. Chem. Res.*, 2019, **52**, 2–11.

6 M. Holzinger, A. Le Goff and S. Cosnier, *Front. Chem.*, 2014, **2**, 63.

7 T. Kawawaki, Y. Negishi and H. Kawasaki, *Nanoscale Adv.*, 2020, **2**, 17–36.

8 Y. Du, H. Sheng, D. Astruc and M. Zhu, *Chem. Rev.*, 2020, **120**, 526–622.

9 L. Liu and A. Corma, *Chem. Rev.*, 2018, **118**, 4981–5079.

10 S. R. K. Perala and S. Kumar, *Langmuir*, 2013, **29**, 9863–9873.

11 V. T. Liveri in *Controlled synthesis of nanoparticles in microheterogeneous systems*, Springer, New York, NY, United states, 1st edn, 2006, pp. 75–91.

12 K. Yamamoto, T. Imaoka, M. Tanabe and T. Kambe, *Chem. Rev.*, 2020, **120**, 1397–1437.

13 V. S. Myers, M. G. Weir, E. V. Carino, D. F. Yancey, S. Pande and R. M. Crooks, *Chem. Sci.*, 2011, **2**, 1632–1646.

14 P. Pachfule, S. Kandambeth, D. Díaz Díaz and R. Banerjee, *Chem. Commun.*, 2014, **50**, 3169–3172.

15 M. Bhadra, H. S. Sasmal, A. Basu, S. P. Midya, S. Kandambeth, P. Pachfule, E. Balaraman and R. Banerjee, *ACS Appl. Mater. Interfaces*, 2017, **9**, 13785–13792.

16 J. Wang, Y. Yu, H. Yu, W. Wang, L.-L. Shen, G.-R. Zhang and D. Mei, *ACS Catal.*, 2023, **13**, 5135–5146.

17 L. Zhang, M. Zhou, A. Wang and T. Zhang, *Chem. Rev.*, 2020, **120**, 683–733.

18 S. Bai, Y. Y. Wang and Y. F. Han, *Chin. J. Chem.*, 2019, **37**, 1289–1290.

19 G. J. Chen, W. L. Xin, J. S. Wang, J. Y. Cheng and Y. B. Dong, *Chem. Commun.*, 2019, **55**, 3586–3589.

20 X. Yang, J. K. Sun, M. Kitta, H. Pang and Q. Xu, *Nat. Catal.*, 2018, **1**, 214–220.

21 J. K. Sun, W. W. Zhan, T. Akita and Q. Xu, *J. Am. Chem. Soc.*, 2015, **137**, 7063–7066.

22 R. McCaffrey, H. Long, Y. Jin, A. Sanders, W. Park and W. Zhang, *J. Am. Chem. Soc.*, 2014, **136**, 1782–1785.

23 B. Mondal, K. Acharyya, P. Howlader and P. S. Mukherjee, *J. Am. Chem. Soc.*, 2016, **138**, 1709–1716.

24 B. Mondal and P. S. Mukherjee, *J. Am. Chem. Soc.*, 2018, **140**, 12592–12601.

25 B. Mondal, P. Bhandari and P. S. Mukherjee, *Chem. - Eur. J.*, 2020, **26**, 15007–15015.

26 S. Y. Zhang, Z. Kochovski, H. C. Lee, Y. Lu, H. Zhang, J. Zhang, J. K. Sun and J. Yuan, *Chem. Sci.*, 2019, **10**, 1450–1456.

27 V. Sharma, D. De, R. Saha, P. K. Chattaraj and P. K. Bharadwaj, *ACS Appl. Mater. Interfaces*, 2020, **12**, 8539–8546.

28 A. Verma, K. Tomar and P. K. Bharadwaj, *Inorg. Chem.*, 2019, **58**, 1003–1006.

29 R. Saha, B. Mondal and P. S. Mukherjee, *Chem. Rev.*, 2022, **122**, 12244–12307.

30 E. H. Peters and M. Mayor, *Chem. Commun.*, 2023, **59**, 4895–4898.

31 Y. Ma, X. Kuang, X. Deng, B. Zi, J. Zeng, J. Zhang, Z. Zhu, Y. Zhang and Q. Liu, *Microporous Mesoporous Mater.*, 2022, **335**, 111701.

32 T. Liu, S. Bai, L. Zhang, F. E. Hahn and Y.-F. Han, *Natl. Sci. Rev.*, 2022, **9**, nwac067.

33 S. Wang, X. Gao, X. Hang, X. Zhu, H. Han, W. Liao and W. Chen, *J. Am. Chem. Soc.*, 2016, **138**, 16236–16239.

34 S. Wang, X. Gao, X. Hang, X. Zhu, H. Han, X. Li, W. Liao and W. Chen, *J. Am. Chem. Soc.*, 2018, **140**, 6271–6277.

35 S. L. Hou, J. Dong, Z. H. Zhu, L. C. Geng, Y. Ma and B. Zhao, *Chem. Mater.*, 2020, **32**, 7063–7069.

36 Y. Fang, Z. Xiao, J. Li, C. Lollar, L. Liu, X. Lian, S. Yuan, S. Banerjee, P. Zhang and H. C. Zhou, *Angew. Chem., Int. Ed.*, 2018, **57**, 5283–5287.

37 Y. Fang, J. L. Li, T. Togo, F. Y. Jin, Z. F. Xiao, L. J. Liu, H. Drake, X. Z. Lian and H. C. Zhou, *Chem*, 2018, **4**, 555–563.

38 X. Hang, S. Wang, H. Pang and Q. Xu, *Chem. Sci.*, 2022, **13**, 461–468.

39 K. Suzuki, S. Sato and M. Fujita, *Nat. Chem.*, 2010, **2**, 25–29.

40 K. Suzuki, K. Takao, S. Sato and M. Fujita, *Angew. Chem., Int. Ed.*, 2011, **50**, 4858–4861.

41 T. Ichijo, S. Sato and M. Fujita, *J. Am. Chem. Soc.*, 2013, **135**, 6786–6789.

42 E. Ubasart, I. Mustieles Marin, J. M. Asensio, G. Mencia, Á. M. López-Vinasco, C. García-Simón, I. del Rosal, R. Poteau, B. Chaudret and X. Ribas, *Nanoscale Horiz.*, 2022, **7**, 607–615.

43 W. L. Jiang, J. C. Shen, Z. Peng, G. Y. Wu, G. Q. Yin, X. Shi and H. B. Yang, *J. Mater. Chem. A*, 2020, **8**, 12097–12105.

44 C. Wang, F. Sun, G. He, H. Zhao, L. Tian, Y. Cheng and G. Li, *Curr. Opin. Colloid Interface Sci.*, 2023, **63**, 101660.

45 J.-Y. Li, X.-D. Yang, F.-X. Chen and J.-K. Sun, *Mater. Chem. Front.*, 2023, **7**, 5355–5376.

46 L.-M. Cao, J. Zhang, X.-F. Zhang and C.-T. He, *Chem. Sci.*, 2022, **13**, 1569–1593.

47 X. Yang and Q. Xu, *Trends Chem.*, 2020, **2**, 214–226.

48 S. Sato, J. Iida, K. Suzuki, M. Kawano, T. Ozeki and M. Fujita, *Science*, 2006, **313**, 1273–1276.

49 K. Harris, D. Fujita and M. Fujita, *Chem. Commun.*, 2013, **49**, 6703–6712.

50 K. Harris, Q.-F. Sun, S. Sato and M. Fujita, *J. Am. Chem. Soc.*, 2013, **135**, 12497–12499.

51 M. Tominaga, K. Suzuki, M. Kawano, T. Kusukawa, T. Ozeki, S. Sakamoto, K. Yamaguchi and M. Fujita, *Angew. Chem., Int. Ed.*, 2004, **43**, 5621–5625.

52 J. Liu, T. Luo, Y. Xue, L. Mao, P. J. Stang and M. Wang, *Angew. Chemie*, 2021, **133**, 5489–5495.

53 X. Yan, P. Wei, Y. Liu, M. Wang, C. Chen, J. Zhao, G. Li, M. L. Saha, Z. Zhou, Z. An, X. Li and P. J. Stang, *J. Am. Chem. Soc.*, 2019, **141**, 9673–9679.

54 Q. Q. Wang, S. Gonell, S. H. A. M. Leenders, M. Dürr, I. Ivanovic-Burmazovic and J. N. H. Reek, *Nat. Chem.*, 2016, **8**, 225–230.

55 F. Yu, D. Poole, S. Mathew, N. Yan, J. Hessels, N. Orth, I. Ivanović-Burmazović and J. N. H. Reek, *Angew. Chem., Int. Ed.*, 2018, **57**, 11247–11251.

56 S. Gonell and J. N. H. Reek, *ChemCatChem*, 2019, **11**, 1458–1464.

57 B. L. Tran, J. L. Fulton, J. C. Linehan, J. A. Lercher and R. M. Bullock, *ACS Catal.*, 2018, **8**, 8441–8449.

58 W. Oberhauser, C. Evangelisti, A. Liscio, A. Kovtun, Y. Cao and F. Vizza, *J. Catal.*, 2018, **368**, 298–305.

59 C. Cerezo-Navarrete, P. Lara and L. M. Martínez-Prieto, *Catalysts*, 2020, **10**, 1144.

60 M. Ghosh and S. Khan, *ACS Catal.*, 2023, **13**, 9313–9325.

61 R. Zaffaroni, E. O. Bobylev, R. Plessius, J. I. Van Der Vlugt and J. N. H. Reek, *J. Am. Chem. Soc.*, 2020, **142**, 8837–8847.

62 M. A. N. Virboul, Sulfonate Functionalisation of Transition Metal Complexes: A Versatile Tool Towards Catalyst Recovery, PhD thesis, Utrecht university, Utrecht, 2011, https://dspace.library.uu.nl/handle/1874/203778, accessed 2023-06-01.

63 Y. Lin and R. G. Finke, *J. Am. Chem. Soc.*, 1994, **116**, 8335–8353.

64 S. K. Samanta, D. Moncelet, V. Briken and L. Isaacs, *J. Am. Chem. Soc.*, 2016, **138**, 14488–14496.

65 C. Gütz, R. Hovorka, C. Klein, Q. Q. Jiang, C. Bannwarth, M. Engeser, C. Schmuck, W. Assenmacher, W. Mader, F. Topić, K. Rissanen, S. Grimme and A. Lützen, *Angew. Chem., Int. Ed.*, 2014, **53**, 1693–1698.

66 X. X. Gou, T. Liu, Y. Y. Wang and Y. F. Han, *Angew. Chem., Int. Ed.*, 2020, **59**, 16683–16689.

67 W. Oberhauser, C. Evangelisti, A. Liscio, A. Kovtun, Y. Cao and F. Vizza, *J. Catal.*, 2018, **368**, 298–305.

68 H. Y. Hall and P. M. A. Sherwood, *J. Chem. Soc. Faraday Trans. 1 Phys. Chem. Condens. Phases*, 1984, **80**, 135–152.

69 C. Crotti, E. Farnetti, S. Filipuzzi, M. Stener, E. Zangrando and P. Moras, *Dalton Trans.*, 2007, 133–142.

70 T. Higaki, H. Kitazawa, S. Yamazoe and T. Tsukuda, *Nanoscale*, 2016, **8**, 11371–11374.

71 P. Brant, L. S. Benner and A. L. Balch, *Inorg. Chem.*, 1979, **18**, 3422–3427.

72 M. J. Sharif, P. Maity, S. Yamazoe and T. Tsukuda, *Chem. Lett.*, 2013, **42**, 1023–1025.